NUREG-0263

AN EXPERIMENTAL STUDY OF THE MOLTEN GLASS/WATER THERMAL INTERACTION

University of California at Los Angeles
for
U. S. Nuclear Regulatory Commission

Available from
National Technical Information Service
Springfield, Virginia 22161
Price: Printed Copy $4.00 ; Microfiche $3.00

The price of this document for requestors outside of the North American Continent can be obtained from the National Technical Information Service.

NUREG-0263
NRC-7

AN EXPERIMENTAL STUDY OF THE MOLTEN GLASS/WATER THERMAL INTERACTION

V. H. Arakeri, I. Catton, and W. E. Kastenberg

Principal Investigators
I. Catton
W. E. Kastenberg

Manuscript Completed: January 1977
Date Published: June 1977

School of Engineering and Applied Science
University of California
Los Angeles, CA 90024

Prepared for
Division of Reactor Safety Research
Office of Nuclear Regulatory Research
U. S. Nuclear Regulatory Commission
Under Contract No. AT(49-24)-0246

PREFACE

This report represents one aspect of the research program "Safety Considerations of Commercial Liquid Metal Fast Breeder Reactors" (AT(04-3) PA223 and AT(49-24)-0246) funded by the U. S. Nuclear Regulatory Commission, Division of Reactor Safety Research. The research program is divided into the following tasks: a) transient analysis of fuel elements, b) accident analysis, c) post accident heat removal, d) fuel-coolant interactions and e) thermodynamic effects.

Reports prepared previously under this grant include the following:

1. Post Accident Heat Removal with Advanced LMFBR Fuels, R. D. Gasser, UCLA-ENG-7518 (March 1975).
2. Dry-Out of a Fluidized Particle Bed with Internal Heat Generation, R. S. Keowen and I. Catton, UCLA-ENG-7519 (March 1975).
3. Laminar Natural Convection from Blunt Bodies with Arbitrary Surface Heat Flux or Surface Temperature, G. M. Harpole, UCLA-ENG-7527 (April 1975).
4. Preliminary Assessments of Carbide Fuel Pins During Mild Overpower Transients, G. M. Nickerson, UCLA-ENG-7582 (October 1975).
5. A Simplified Method of Computing Clad and Fuel Strain and Stress During Irradiation, Y. Sun and D. Okrent, UCLA-ENG-7591 (Part I) (October 1975).
6. An Experimental Study of the Thermal Interaction for Molten Tin Dropped into Water, V. M. Arakeri, I. Catton, W. E. Kastenberg and M. S. Plesset, UCLA-ENG-7592 (December 1975).
7. A Mechanistic Study of Fuel Freezing and Channel Plugging During

Fast Reactor Overpower Excursions, V. K. Dhir, K. Wong and W. E. Kastenberg, UCLA-ENG-7679 (July 1976).

8. A Simulation of Thermal Phenomenon Expected in Fuel Coolant Interactions in LMFBR's, J. Yasin, UCLA-ENG-76100 (September 1976).
9. On the Nonequilibrium Behavior of Fission Gas Bubbles with Emphasis on the Effects of Equation of State, W. G. Steele, UCLA-ENG-76118 (December 1976).
10. A Method for the Determination of the Equation of State of Advanced Fuels Based on the Properties of Normal Fluids, M. J. Hecht, UCLA-ENG-76112 (December 1976).
11. A Simplified Method of Computing Clad and Fuel Strain and Stress During Irradiation, Y. Sun and D. Okrent, UCLA-ENG-7705 (Part II) (January 1977).
12. Natural Convection in Horizontal Fluid Layers, A. J. Suo-Anttila and I. Catton, UCLA-ENG-7706 (January 1977).

ABSTRACT

Molten glass interacts explosively with water under certain contact mode conditions. The contact mode found explosive is as follows: molten glass enters the water bath in the film boiling regime (as predicted by Henry's correlation) and soon after entry, the vapor film is perturbed sufficiently by an external pressure pulse. The ensuing reaction proceeds basically along the same lines as energetic tin/water interactions observed by several investigators. In the absence of this pressure pulse, the event is non-energetic.

The present findings are for a combination ir which the hot material has a very low thermal diffusivity and the calculated interface temperature is significantly ($\sim$175° C) below its melting temperature. This is similar to the characteristics of the UO_2/sodium combination. The observed explosive glass/water interactions show growth times of the order of a few milliseconds. The particulate size distribution from the present tests was coarser than the particulate size distribution from some in-pile and out-of-pile UO_2/sodium interaction tests.

TABLE OF CONTENTS

LIST OF FIGURES

LIST OF TABLES

I. INTRODUCTION

Molten fuel/coolant, thermal interactions are an important aspect in the analysis of whole core disruptive accidents for Liquid Metal Fast Breeder Reactors (LMFBR's). To understand the true nature of fuel/coolant interactions, several experimental and theoretical studies have been initiated in many laboratories [1]. To date, the experimental results for molten UO_2/sodium indicate two important trends. First, the UO_2/sodium interaction is not of a violent or explosive nature. Second, post-experimental examination of the fuel debris indicates a large degree of fragmentation or surface enhancement. A similar degree of fragmentation has been observed for molten metal/water tests; however, the thermal interactions in these tests [2] have been of violent or explosive nature.

The discrepancy noted, among others, may be as a result of completely differing thermal properties of both the fuel and coolant for metal/water and UO_2/sodium combinations. The differences are clear from the comparison of thermal properties presented in Table 1.

The predicted minimum temperature for film boiling is based on Henry's [4] correlation. Some of the predicted temperatures for various fuel/coolant combinations are presented in Table 2. The liquid/liquid contact may take place as a result of the onset of transition boiling under natural conditions or as a result of the forceful disturbance of the vapor film by external means. In any event, the predicted interface temperatures for reactor fuel/sodium combinations are considerably lower than the melting temperatures of the fuels. On the other hand, for the case of the tin/water combination, quite the contrary is true. The predicted interface temperature is considerably above the melting temperature of tin and it may be noted here that tin has been used extensively

TABLE 1.

Thermal Properties of Some Fuels.

Fuel	ρKC Cal^2/cm^4 sec deg^2	C Cal/gm deg	α cm^2/sec
Reactor materials			
UO_2	0.006	0.11	0.005
UC	0.05	0.084	0.056
UN	0.065	0.09	0.066
SS	0.091	0.159	0.06
Simulant materials			
Sn	0.036	0.078	0.13
Al	0.17	0.259	0.49
AgCl	0.001	0.076	0.005
Glass*	0.003	0.435	0.0014

*Value is for molten B_2O_3 [3]

TABLE 2.

Thermal Characteristics of Some Fuel/Coolant Combinations.

Fuel/coolant combination	$a\sqrt{\frac{\rho KC}{(\rho KC)C}}$	T_{mf} °C	T_I °C	T_{mfb} °C
UO_2 (3,000° C)/Na (400° C)	0.334	2,800	1,051	12,000
UC (3,000° C)/Na (400° C)	1.07	2,530	1,744	7,765
UN (3,000° C)/Na (400° C)	1.23	2,860	1,834	6,960
SS (3,000° C)/Na (400° C)	1.45	1,427	1,940	4,810
Sn (800° C)/H_2O (20° C)	6.0	231.9	688	506
Al (800° C)/H_2O (20° C)	13.0	660	745	265
AgCl (800° C)/H_2O (20° C)	1.0	455	410	1,195
Glass (900° C)/H_2O (20° C)	1.7	750	570	425

Notes: T_{mf} is the melting temperature of the fuel.

T_I is the interface temperature.

T_{mfb} is the minimum temperature for film boiling from Henry's correlation.

as a simulant fuel for many experimental studies concerning fuel/coolant interactions. In addition, experimental observations of tin/water interactions have been the basis of a recently proposed hypothesis [5, 6] for fuel/coolant interaction and has received considerable attention. The proposed model [5] involves the following stages for the development of an explosive fuel/coolant interaction:

(a) At the instant of liquid/liquid contact a vapor bubble is formed at the fuel surface which grows into the subcooled region of the coolant.

(b) Due to condensation, the vapor bubble collapses; however, the collapse is asymmetric due to the pressure of the liquid or solid fuel surface. This results in a high velocity jet as predicted by Plesset and Chapman [7] for cavitation bubble collapse.

(c) The jet of coolant penetrates the fuel and due to its high velocity disintegrates causing rapid increase in the fuel coolant contact area.

(d) As the jet of coolant penetrates and breaks up, heat is rapidly transferred from the hot surrounding fuel to the coolant.

(e) When the jet has been heated to a certain temperature it suddenly vaporizes to form a high pressure vapor bubble. The rapid expansion of this bubble results in the dispersal of the fuel into the coolant.

(f) A new vapor bubble is formed and the process repeats from stage (a).

The use of this model to predict UO_2/sodium behavior requires the

assumptions that a coolant jet is able to penetrate a solidified crust at the surface and rapid heat transfer is possible from a hot surrounding fuel of low thermal diffusivity to the coolant. Buchanan [8] has demonstrated the possibility of coolant jet penetration of a solidified crust theoretically; however, to the authors' knowledge, no experimental observations of interactions involving simulant fuels which show the possibility of crust formation upon liquid/liquid contact have been made. Therefore, the goal of this experimental work was to study the fuel/coolant interaction by using a simulant fuel which has a low thermal diffusivity and allows the possibility of crust formation based on interface temperature calculations upon liquid/liquid contact. Examination of Tables 1 and 2 clearly show that molten glass* would be a very suitable simulant fuel. The use of molten AgCl is also a possibility, but the predicted interface temperature for the AgCl/water combination is only slightly below that of the melting temperature of AgCl. Hence, the use of molten glass over molten AgCl was preferred. In addition, it was decided to study molten glass/water interactions under both "natural" and "forced" free fall conditions. This decision was based on the possibility that molten glass may solidify significantly prior to the vapor film breakdown under natural free fall conditions because the predicted temperature for film boiling by Henry's correlation (Table 2) is considerably lower than the melting temperature of glass.

In Section II, experimental methods will be described with emphasis on the making of the test glass for the present work and the use of an exploding wire as a technique of disturbing the vapor film surrounding the hot molten material. In Section III, results will be presented which

*Estimated homogenous crystallization temperature for glass based on the method noted in Ref. [9] is only about 10° C below the melting point of glass.

include the study of exploding wire phenomena underwater and the initial tests which show the effectiveness of a wire explosion to trigger an interaction for glass/water combinations. In Section IV, the findings are discussed with particular emphasis on the meaning of present findings as related to UO_2/sodium tests. Finally the conclusions based on present findings are noted in Section V.

II. EXPERIMENTAL PROCEDURE

A. General Description. The details of the test chamber utilized for the present work may be found in Reference [2]. Basically the chamber consists of two sections. The upper section contains the graphite crucible in which the metal or glass is heated by two half-circular electrical heaters. The lower section contains regular tap water which acts as the coolant medium. The lower section also contains the glass windows for light illumination and photographic purposes.

Multiflash photographs of the event were obtained by using two stroboscopes as light sources. The flashing rate and duration of the stroboscopes was controlled externally so that 20 to 25 frames could be recorded on a 10 cm by 12.7 cm sheet film rotating at the image plane. The flashing of the stroboscopes was synchronized with the arrival of the molten hot material at the window level by the use of an external delay circuit. Further details of the present photographic technique may also be found in Reference [2]. It may, however, be noted here that the typical rotation speed required to record about twenty frames (1.27 cm by 1.27 cm size) at one thousand frames per second was 1,725 RPM.

The temperature of the hot material was measured with a chrome-alumel thermocouple. Temperature of the water bath was measured with a single copper constantan thermocouple. To avoid temperature stratification in the coolant bath, water was stirred with the help of an external pump a few minutes prior to the dropping of the hot material. Pressure measurements were made with a Cebesco model LC-10 hydrophone. The sensivity, with the cable, of this transducer is quoted by the manufacturer to be 2-78 volts per bar. The output of the transducer was photographed from a dual trace oscilloscope.

B. Test Glass. The following two requirements were considered in selecting the proper glass:

(a) relatively low melting temperature (∿700° C), and

(b) relatively fluid at test temperature (∿700° C).

Initially, glazing material, which is a lead-based glass and has a relatively low melting temperature, was tried. However, at test temperature, this glass was very sticky and great difficulties were encountered in dropping the molten glass from the graphite crucible by pulling of the shuttle. Similar difficulties were experienced when lead-based silica glasses were tried. From further experimentation with various combinations of base materials for the making of glass, it was found that the combination of B_2O_3 and PbO would be suitable. High PbO content glass, which had a relatively low melting point, interacted with the graphite crucible at high temperatures, turning from an originally yellow color to black. However, use of 60% B_2O_3 and 40% PbO (by weight) proved to be a very suitable combination. The melting point of this combination was found* to be about 750° C and at a temperature of 900° C the molten glass was almost as fluid as water at room temperature. In addition, this combination of glasses did not interact with the graphite crucible to a great extent and freely dropped from the crucible upon the pulling of the shuttle.

The glass itself was prepared by thoroughly mixing pre-weighed powdered forms of B_2O_3 and PbO in a porcelain crucible. This mixture was fused by placing the crucible in an oven pre-heated to 1,000° C. The mixture was left in the oven for about ten minutes at this temperature. Intermittently the crucible was removed and turned around manually to

*See also Reference [3].

assure further mixing of the components in the molten state. After ten minutes the resulting molten mass was poured onto a graphite block for cooling. The final physical appearance of the molten mass was in the form of a milky to clear white glassy mold. This solidified and cooled glass was used as test specimen for dropping experiments. Several batches of this glass each weighing twenty-five grams were prepared separately at a given time. However, from initial dropping tests it was found that only the central core of the molten glass, weighing about 12 to 15 grams, fell as a single drop immediately after pulling of the shuttle.

C. Pressure Pulse Generation. Some methods of pressure pulse generation in the coolant are noted in Reference [10]. For the present work, all of these were considered, but finally due to simplicity it was found suitable to use the technique of exploding a thin wire underwater as a source of pressure pulse in the coolant. First the effectiveness of the technique was tested on a tin/water combination (which is known to produce explosive interactions even under natural free fall conditions). As will be shown later, the results were promising and it was felt that the technique should be effective for glass/water combinations also.

Detailed studies of the techniques of exploding a thin wire in air have been conducted by several workers [11]. In principle similar techniques can also be utilized for exploding a thin wire underwater. In the present experiments, the two electrical terminals were formed by bringing two insulated copper wires (3.2 mm diameter) from the bottom of the test chamber. The two terminals were placed 3.8 cm apart and were normally brought up to the lower level of the glass windows. For the purpose of photographing the underwater explosion of a thin wire, the two terminals in the latter position are shown in the first frame of Figure 1(A). Also

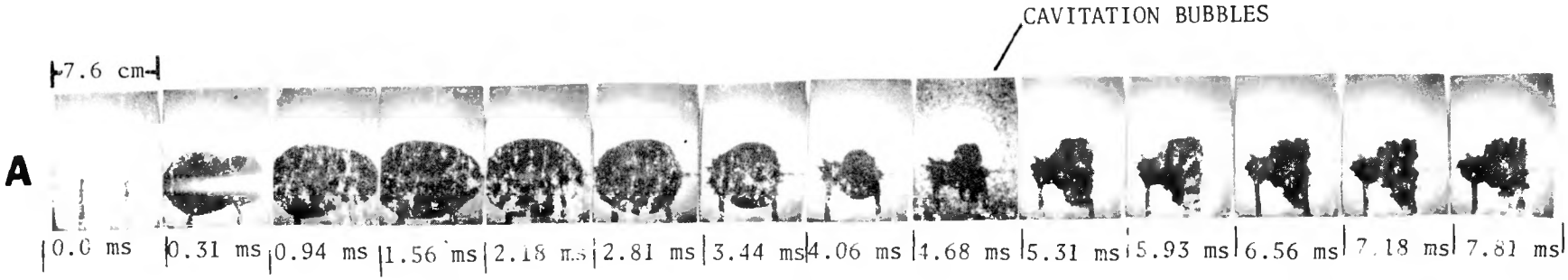

(A) Sequence of photographs illustrating the "bubble" growth and collapse cycles.

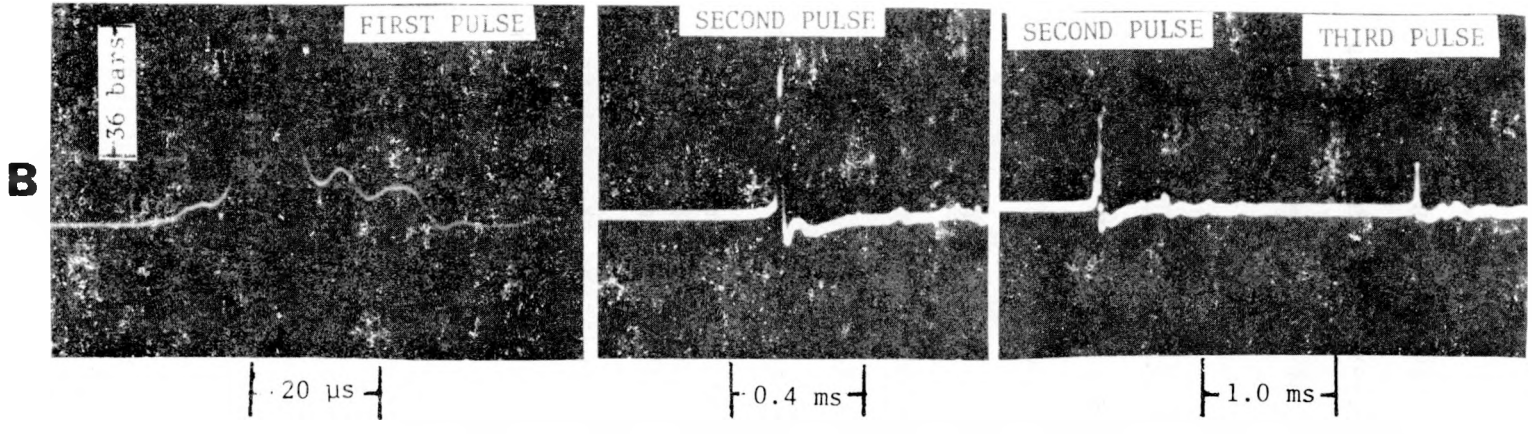

(B) Pressure levels of three pulses resulting from single explosion. Transducer ~4.3 cm away.

FIGURE 1. Wire Explosion Observations.

seen in the same frame is a thin copper wire of 0.254 mm diamter soldered across the two terminals. This thin wire was exploded by discharging three twenty-five microfarad capacitors connected in parallel, and nominally charged to two kilo-volts. The discharge across the terminals was initiated by closing a four pole relay switch. The relay switch was closed by activation of a regenerative circuit which could be triggered with a small amplitude voltage pulse. The time period between triggering of the regenerative circuit and initiation of the flashing of the stroboscopes could be controlled with an external delay circuit. Thus, with this arrangement it was possible to photograph the events prior to and after the explosion of the thin wire.

Multiflash photographs of the "bubble" created in water by the explosion of the wire were recorded at 1,600 frames per second by the photographic technique noted earlier. Pressure pulse measurements were made with the LC-10 hydrophone and the oscilloscope used to observe and record the output of the hydrophone was triggered with a photocell which was activated by the light emitted from the exploding wire. With this method of triggering the oscilloscope it was possible to study the initial pressure pulse generated by the exploding wire in some detail.

D. Test Conditions. All of the molten glass/water tests were conducted with initial glass temperature of 880° C and uniform water bath temperature of 22° C. The molten tin/water tests were conducted with initial tin temperature of 785° C and uniform water bath temperature of 27° C. Both molten tin and glass were dropped from a height of 11.25 cm into the water bath, which was about 25 cm in depth. In order to minimize oxidation, the melting of the glass and tin was done in the presence of a constant supply of argon gas.

III. EXPERIMENTAL RESULTS

A. Pressure Pulse Generation by Exploding Wire. From the transducer measurements, it was observed that wire explosions resulted in more than one pressure pulse within the coolant bath. Typically three pressure pulses with decreasing amplitudes and with time delays of the order of milliseconds were noted. From the dimensions of the test chamber it is clear that the multiple pressure pulses were not a result of reflections from either the free surface or the solid surfaces of the test chamber. Photographic studies of the wire explosion indicated that the multiple pressure pulses were a result of growth and collapse cycles of the "bubble" created by the final products. A sequence of photographs illustrating the presence of growth and collapse cycles is shown in Figure 1(A).

From Figure 1(A), it may be seen that the bubble growth is not quite spherically symmetric; however, no instabilities are evident at the boundaries are quite evident, especially in the final stages. The first collapse appears to be complete within about 5 msec of wire explosion and regrowth of the bubble takes place for about 1.5 msec; the second collapse is not quite so evident as the first one. Additional growth and collapse cycles, if existing, were not apparent from the photographs.

Pressure pulse recordings with a transducer located directly above the exploding wire and at a distance of 4.3 cm are shown in the photographs of Figure 1(B). It may be seen from the first photograph of Figure 1(B) that the peak of the first pulse occurs about 32 μsec after the emission of the light from the exploding wire. However, the arrival time of the pressure pulse to the transducer, from the wire, is estimated to be about 20 μsec. Therefore, the first pulse must be emitted only a

few microseconds after the instant of light emission from the exploding wire. The magnitude of the first pulse is seen to be about 50 bars and time duration of the pulse to be about 10 microseconds. The magnitude of the first pulse was observed to fall off as the transducer was moved away from the exploding wire. Measurements with the transducer located at four different distances of 2.54 cm, 4.3 cm, 7.6 cm, and 10.2 cm are shown in Figure 2. The plot shows peak pressure amplitude versus the inverse of the distance from the exploding wire to the transducer tip. For the distances of interest in the present experimental work, the peak pressure amplitude of the first pulse may be taken to be proportional to 1/k and the constant of proportionality to be 265 (Figure 2) with pressure in bars and ℓ in cm. It may be expected that similar behavior will be true for peak pressure amplitudes of the secondary pulses. The constant of proportionality may be estimated from the magnitudes of the secondary pulses measured at one distance of 4.3 cm from the exploding wire to the transducer (Figure 3).

Also shown in Figure 3 are times corresponding to the presence of the secondary pressure pulses within the water bath due to the wire explosion. Comparison of these times with the estimated time (shown in Figure 3) of the maxima and minima of the bubble growth from the photographs of Figure 1(A) strongly indicates that the secondary pulses are emitted at the time of the final stages of the bubble collapse. The first collapse being intense, results in a strong second pulse (40 to 50 bars), whereas the second collapse, being not so intense, results in a relatively weak third pulse ($\sim$12 bars). The reflection of a strong second pulse from the free surface is seen to produce cavitation bubbles within the water. This is shown in one of the frames of Figure 1(A).

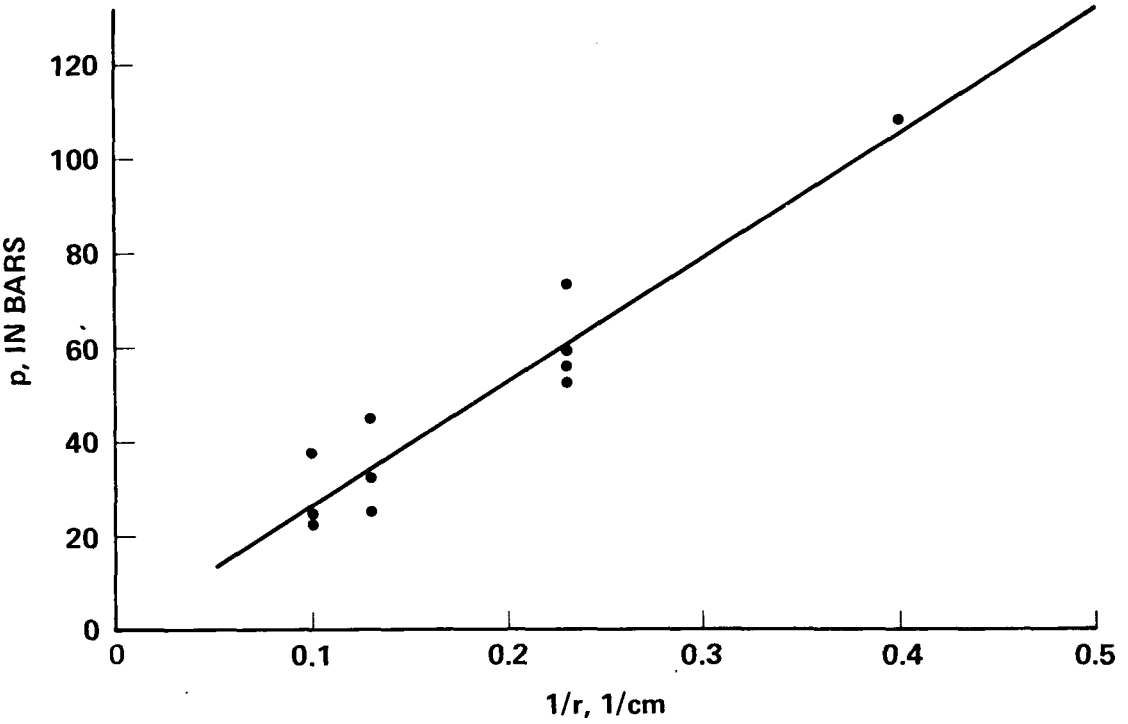

FIGURE 2. Dependence of Magnitude of First Pressure Pulse with Distance.

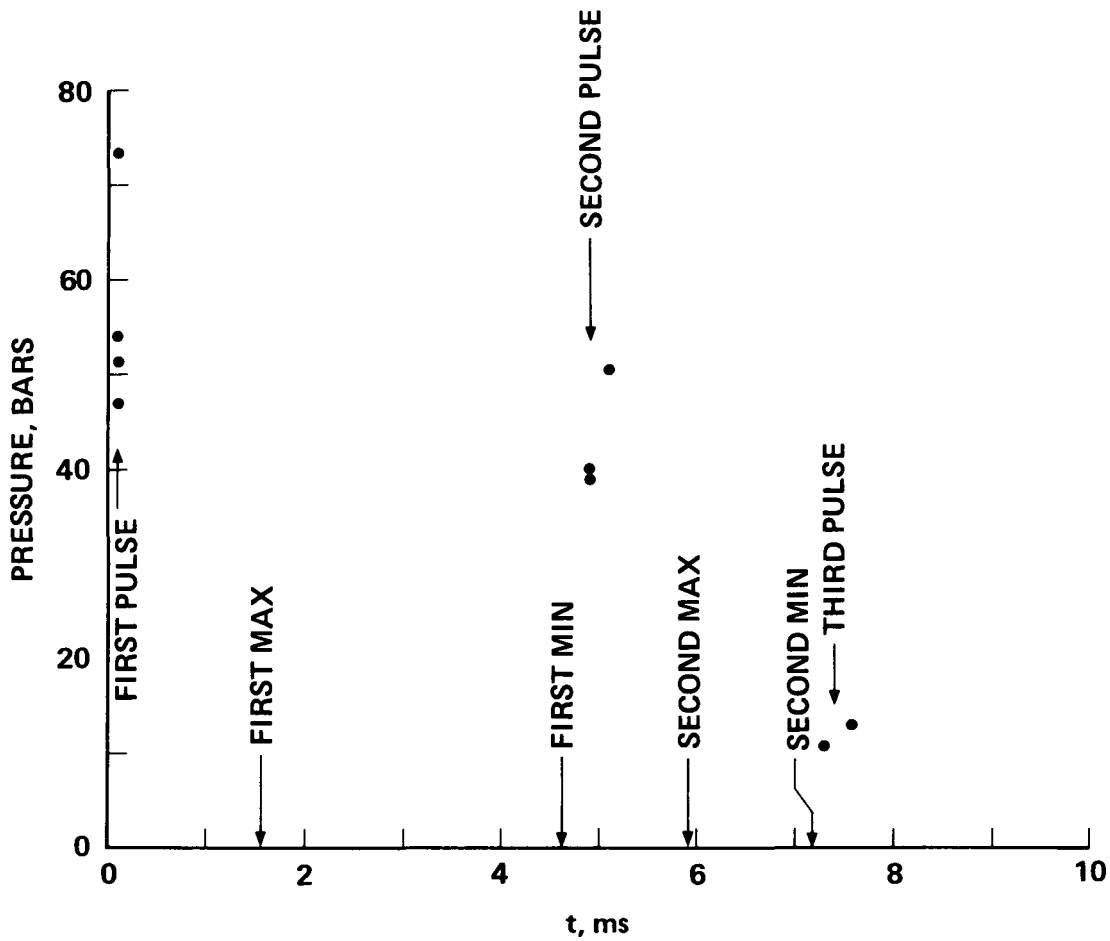

FIGURE 3. Comparison of Times of Secondary Pulses with the Times of Growth Cycles of the "Bubble" Shown in Figure 1(A).

It may be noted here, that since the transducer was located directly above the exploding wire, the measurements shown in Figures 2 and 3 are pressure pulse magnitudes and times as seen by the molten glass or metal under free fall conditions.

B. Forced Tin/Water Interaction. Multiflash photographs of the interaction of molten tin dropped into water are presented in Figures 4(A) and 4(B). The first four frames in each sequence of photographs were taken prior to the explosion of the wire. At the instant of wire explosion, a bright blue flash of light was emitted which illuminated the entire test chamber. The exposure of a frame from this light could easily be distinguished from the exposure of the remaining frames by the light from the stroboscopes. From this, it was possible to estimate the time at which the wire explosion took place. These times are marked on the sequence of photographs of Figures 4(A) and 4(B).

It is clear from Figure 4(A) that the disturbance from the first pressure pulse is sufficient to trigger a strong interaction between molten tin and water within one millisecond of wire explosion. Growth and collapse cycle of this interaction region is observed to continue for the next three frames. Similarly, in Figure 4(B) an interaction between molten tin and water is triggered within two milliseconds of the instant of wire explosion. In both cases the final debris was scattered at the bottom of the test chamber in powder form with fine porous fragmentation. It may be noted here that similar fragmentation with a spontaneous (without external disturbance) tin/water interaction was also observed previously [2]. Further, in the same study it was noted that fragmentation of the above nature was accompanied with strong pressure pulses within the coolant bath. In the present study, however, it was difficult to

(A) and (B) Photographs illustrating the interactions triggered by wire explosion.

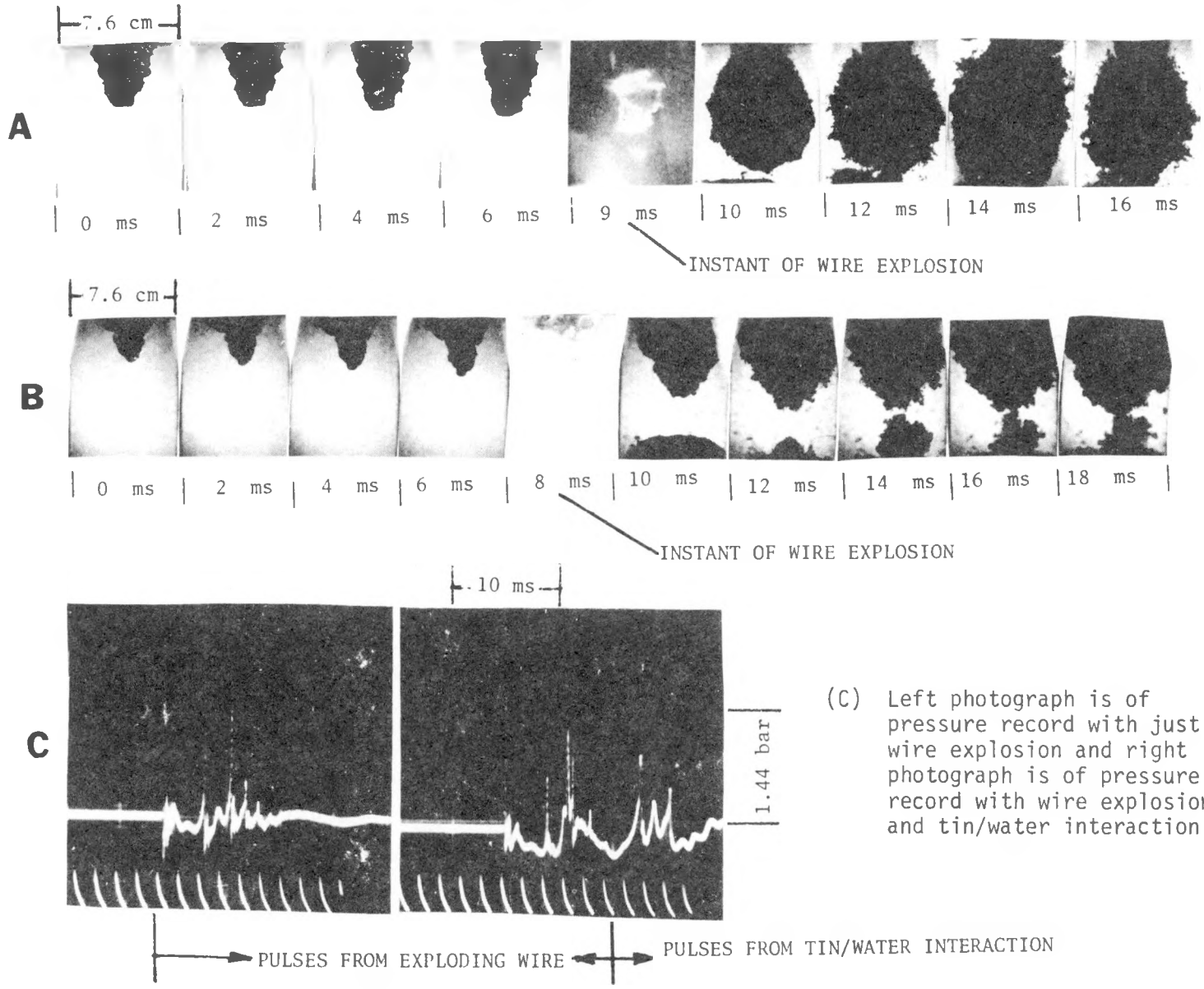

(C) Left photograph is of pressure record with just wire explosion and right photograph is of pressure record with wire explosion and tin/water interaction.

FIGURE 4. Forced Tin/Water Interactions.

sort out the pressure pulses measured from the tin/water interaction from those of the wire explosion itself.

The only possible method of sorting out was by comparing the pressure pulse photograph obtained with just the wire explosion, with the pressure pulse photograph obtained with the wire explosion and the tin/water interaction, such as the comparison for the test conditions of Figure 4(B) as shown in Figure 4(C). The left photograph shows that the pressure pulses due to wire explosion only are damped out within a time period of 10 msec (see also Figure 3). In the right photograph the pressure pulses from the exploding wire are again present; but a delayed (> 10 msec) strong pressure pulse is also seen which is interpreted to be due to the tin/water interaction. If the pressure pulse due to a tin/water interaction is emitted within a time period of 10 msec of wire explosion, then it would be difficult to distinguish it from the pressure pulses recorded from the wire explosion. Such was the case for the test conditions shown in Figure 4(A).

In any case, even through the sorting out of pressure pulses poses a difficulty, the wire explosion is an effective means of disturbing the existing vapor film to trigger an interaction.

C. Natural Glass/Water Interaction. Multiflash photographs of molten glass initially at a temperature of 880° C dropped into water at 22° C are shown in Figure 5(A). The photographs clearly show that no interaction takes place between the two under these contact conditions. The photograph of the final debris confirms this observation. Very little fragmentation of the final debris is observed. However, if a small portion of the final product was pressed between the fingertips, the tendency was to crumble into several smaller pieces, strongly indicating extensive internal cracking.

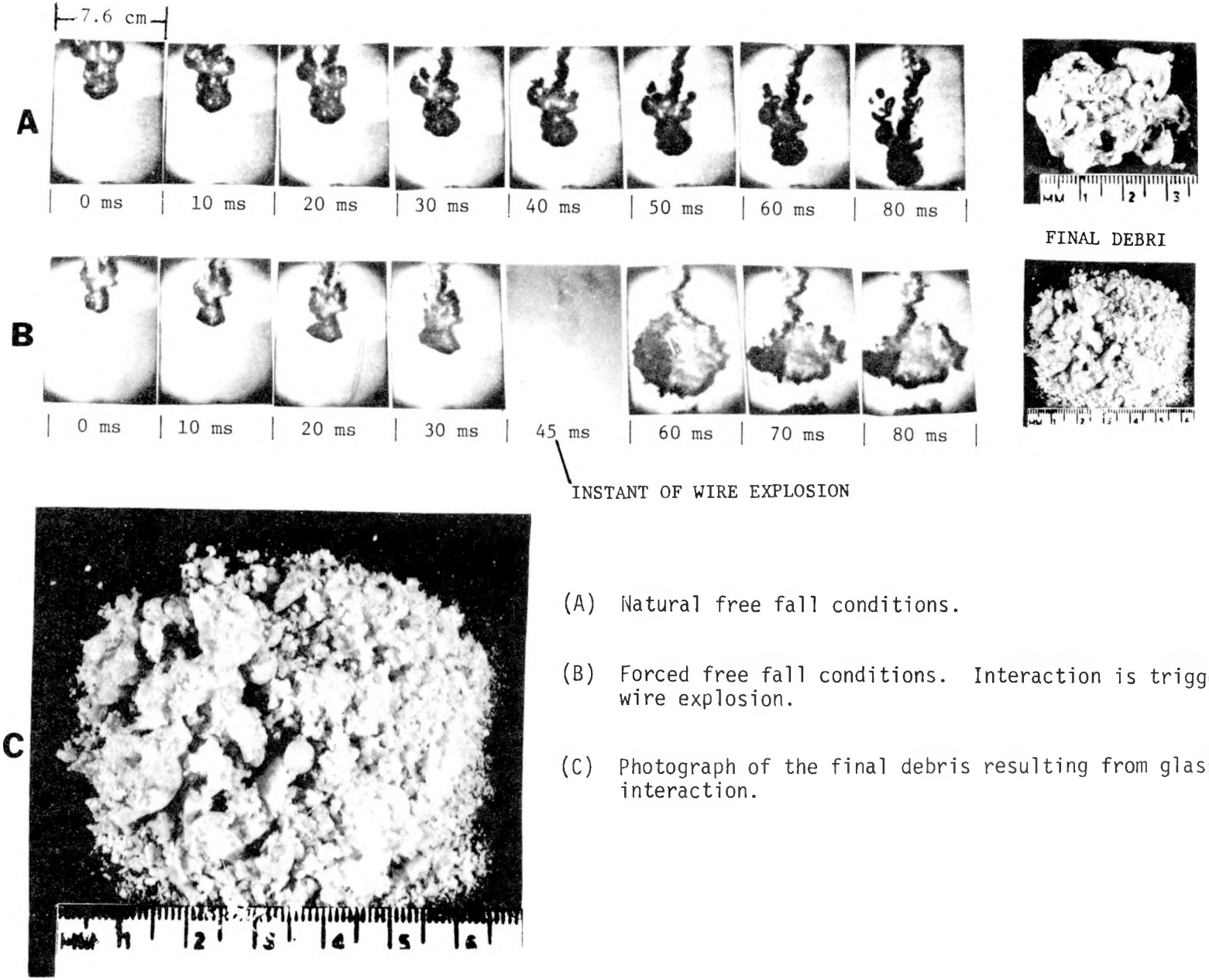

(A) Natural free fall conditions.

(B) Forced free fall conditions. Interaction is triggered by the wire explosion.

(C) Photograph of the final debris resulting from glass/water interaction.

FIGURE 5. Thermal Interaction of Glass/Water.

D. Forced Glass/Water Interaction. A sequence of multiflash photographs for identical initial conditions as for Figure 5(A) is shown in Figure 5(B). However, in the latter case a wire was exploded by the time the molten glass reached the middle level of the window. The frame illuminated by the light from the wire explosion is marked on the sequence of photographs. The next recorded frame (approximately 15 msec after the wire explosion) shows a strong interaction between molten glass and water. Photographs of the final debris confirm this observation in the sense that significant fragmentation has resulted from the interaction. A more detailed photograph of the same debris is shown in Figure 5(C). It is clear from this photograph that fragmentation with a broad particle size distribution has taken place.

Further details of the glass/water interaction triggered by the wire explosion are shown in the sequence of multiflash photographs presented in Figure 6. These photographs were taken at 950 frames per second as compared to only 100 frames per second for the photographs presented in Figure 5(B). The first frame shows the state of molten glass dropped into water prior to the application of external disturbance. The second frame shows the molten glass as illuminated by the light from the wire explosion. The third frame shows the state of molten glass with a surrounding vapor film after it has been disturbed by the first pressure pulse from the wire explosion. Clearly no single large interaction is triggered immediately by the first pulse; however, the vapor interface is not quite as smooth as that observed in the first frame. In the fifth frame, a small interaction is observed in the lower right hand corner. Collapse of this interaction, indicated in the sixth frame and perhaps coupled with the arrival of the second pulse from the wire explosion,

seems to trigger a strong interaction by the seventh frame.

This interaction first grows and then collapses, as is evident from the next four subsequent frames. After the collapse, a second interaction is indicated in the twelfth frame and the collapse of this second interaction seems to result in a third interaction by the fifteenth frame. The growth of the third interaction is quite prominent in the top upper portion of the initial interaction region. No further interactions were evident in the subsequent frames after the growth and collapse of the third interaction. The final debris showed significant fragmentation and the appearance of the final product was very similar in nature to that shown in Figure 5(C).

A pressure transducer trace for the event just described is shown in the lower right photograph of Figure 6. The trace shows pressure pulses from both the wire explosion and the glass/water interaction. This can be inferred by comparing the right photograph with the left one, which shows a pressure pulse recording from just the wire explosion. The two additional pulses in the right photograph can be further identified with the second and third interactions noted in the multiflash photograph sequence of Figure 6. The pressure pulse resulting from the first interaction could not be isolated, since the interaction occurred within the time period of the damping of pressure pulses resulting from the wire explosion.

Another sequence of multiflash photographs showing the glass/water interaction triggered by wire explosion is illustrated in Figure 7(A). As may be seen from the second frame, the molten glass is closer to the source of wire explosion ($\sim$2 cm) than was the case ($\sim$3.5 cm) for the sequence of photographs shown in Figure 6. For this reason, perhaps,

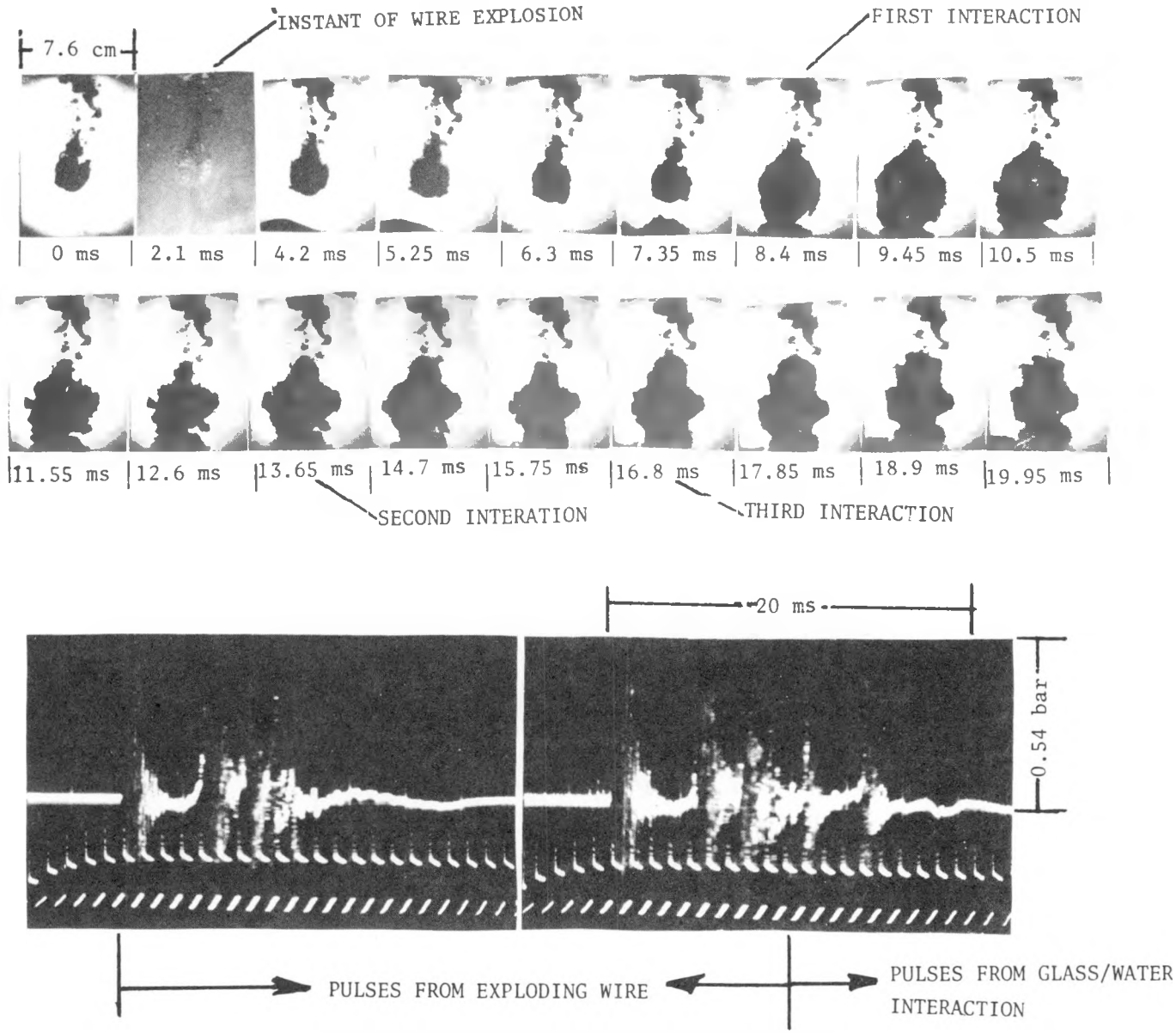

FIGURE 6. Sequence of Multiflash Photographs Illustrating the Growth and Collapse Cycles of the Glass/Water Interaction. Also Shown Are Pressure Recordings of Wire Explosion with and without the Glass/Water Interaction.

the first pressure pulse from the wire explosion itself is able to trigger a relatively strong interaction between glass and water, as may be seen from the third frame. The collapse of the first interaction region is seen to take place in the sixth frame. This results in a second interaction by the next frame. In subsequent frames only a small third interaction in the upper right-hand corner could be identified. The pressure pulses resulting from the second and third interactions could again be distinguished from the pressure pulses resulting from the wire explosion, and this is shown in Figure 7(C).

E. Particle Size Distribution. The interaction shown in the photographs of Figure 7(A) resulted in extensive fragmentation of glass. The final debris, separated into various sized particles, is shown in the photographs of Figure 7(B). The separation was carried out by using hand held sieves of different mesh size. This process had to be carried out very gently since the fragmented particles were extremely fragile. Similar particle size separations were carried out for final debris collected from three additional runs. The fragmented particles in each size group were then weighed separately and the results are shown in Table 3.

The results from Table 3 are shown graphically in Figure 8. Also shown in the same Figure is the range of data from some in-pile and out-of-pile tests conducted with molten UO_2 and sodium. The data is taken from Reference [2], and present results are close to the coarse range of particle size distribution for UO_2/sodium tests.

F. Particle Characteristics. Further analysis of particles shown in Figure 7(B) was conducted using scanning electron microscope photography. Magnified photographs of particles in three ranges of sizes are shown in Figure 9. In Figure 9(a) it may be seen that the particles from 2,362 μ

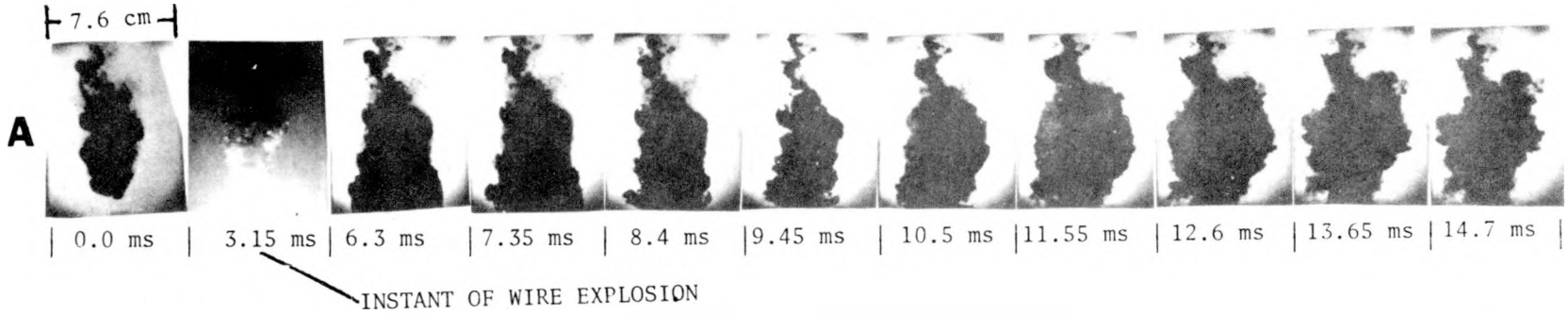

(A) Sequence of multiflash photographs.

(B) Particles from the final debris separated into different size ranges.

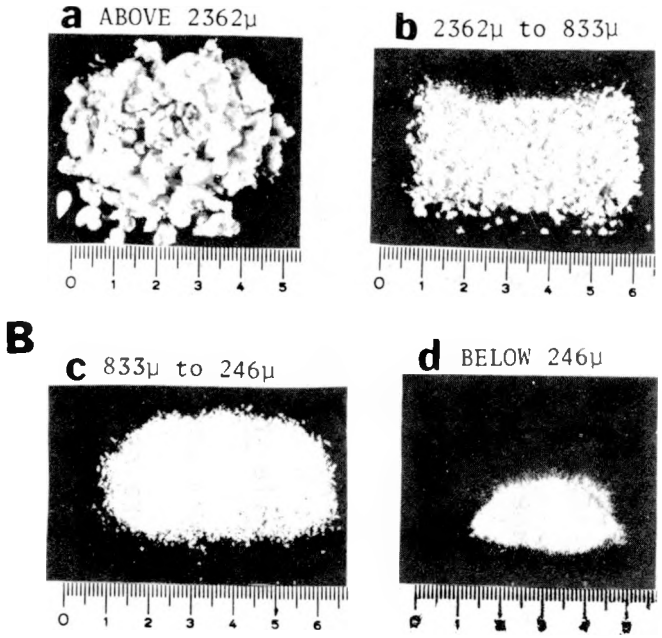

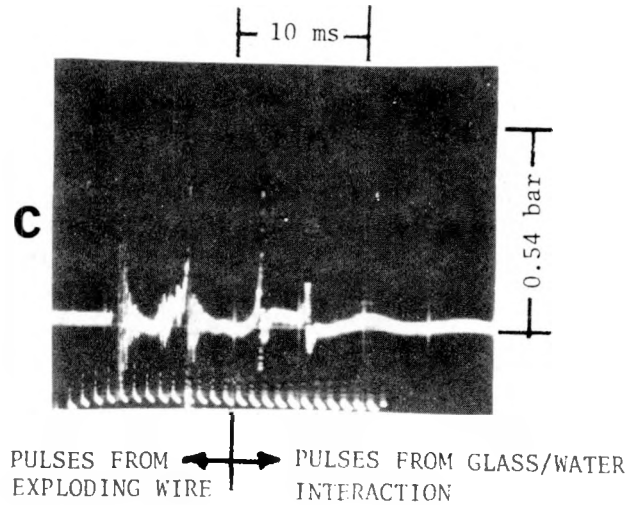

(C) Pressure trace from wire explosion and glass/water interaction.

FIGURE 7. Photographs Illustrating the Glass/Water Interaction.

TABLE 3.

Particle Size Distribution for Glass/Water Interaction Tests.

Range of Particle Size (μ) / Test run no.	Below 246 μ		246 to 833 μ		833 to 2,362 μ		Above 2,362 μ	
	Average particle diameter*	Wt. %	Average particle diameter†	Wt. %	Average particle diameter†	Wt. %	Average particle diameter**	Wt. %
69	200	2.4	540	11.2	1,595	23.2	5,180	55.3
70 [Figure 5(b)]	200	1.34	540	8.0	1,595	24.5	5,180	55.1
72 [Figure 7(A)]	200	2.0	540	11.3	1,595	24.8	5,180	52.8
76 [Figure 6]	200	1.3	540	6.6	1,595	23.7	5,180	56.4

*Arithmetic mean between 250 and 150, since few particles had a diameter less than 150 μ.

†Arithmetic mean between 250, 830 and 2,360 is taken.

**Arithmetic mean between 2,360 and 8,000, since few particles had a diameter greater than 8,000 μ.

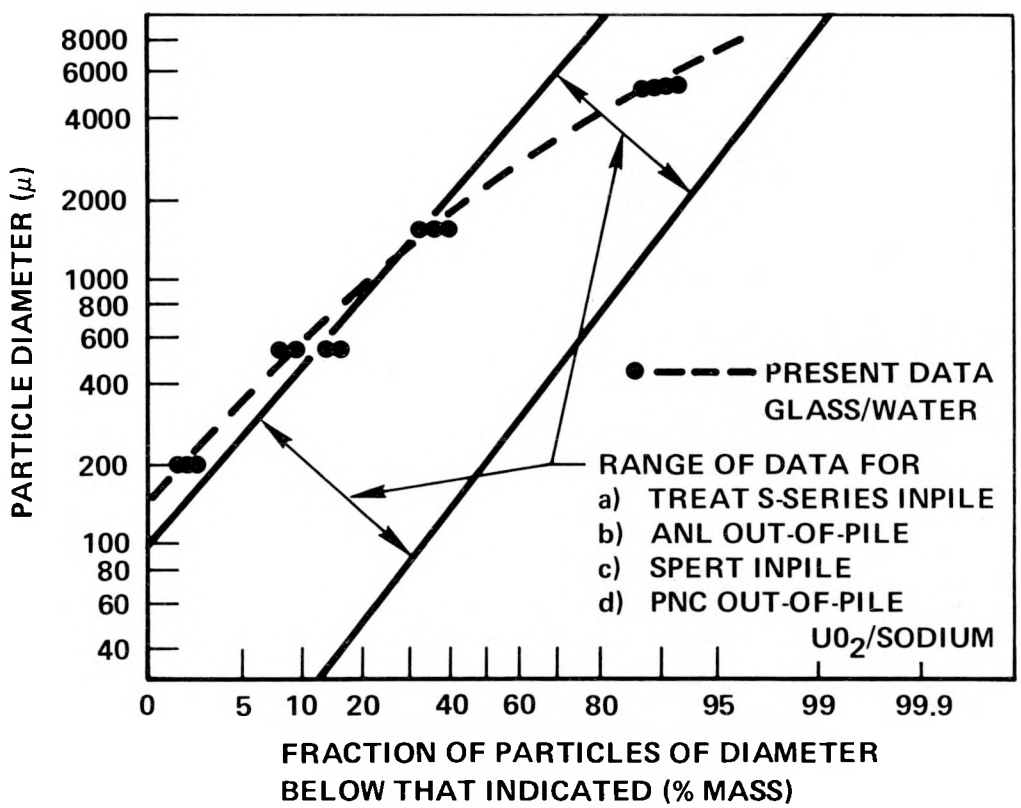

FIGURE 8. Comparison of Particle Size Distribution from Present Glass/Water Interactions with the Range of Particle Size Distribution from some UO_2/Sodium Interactions.

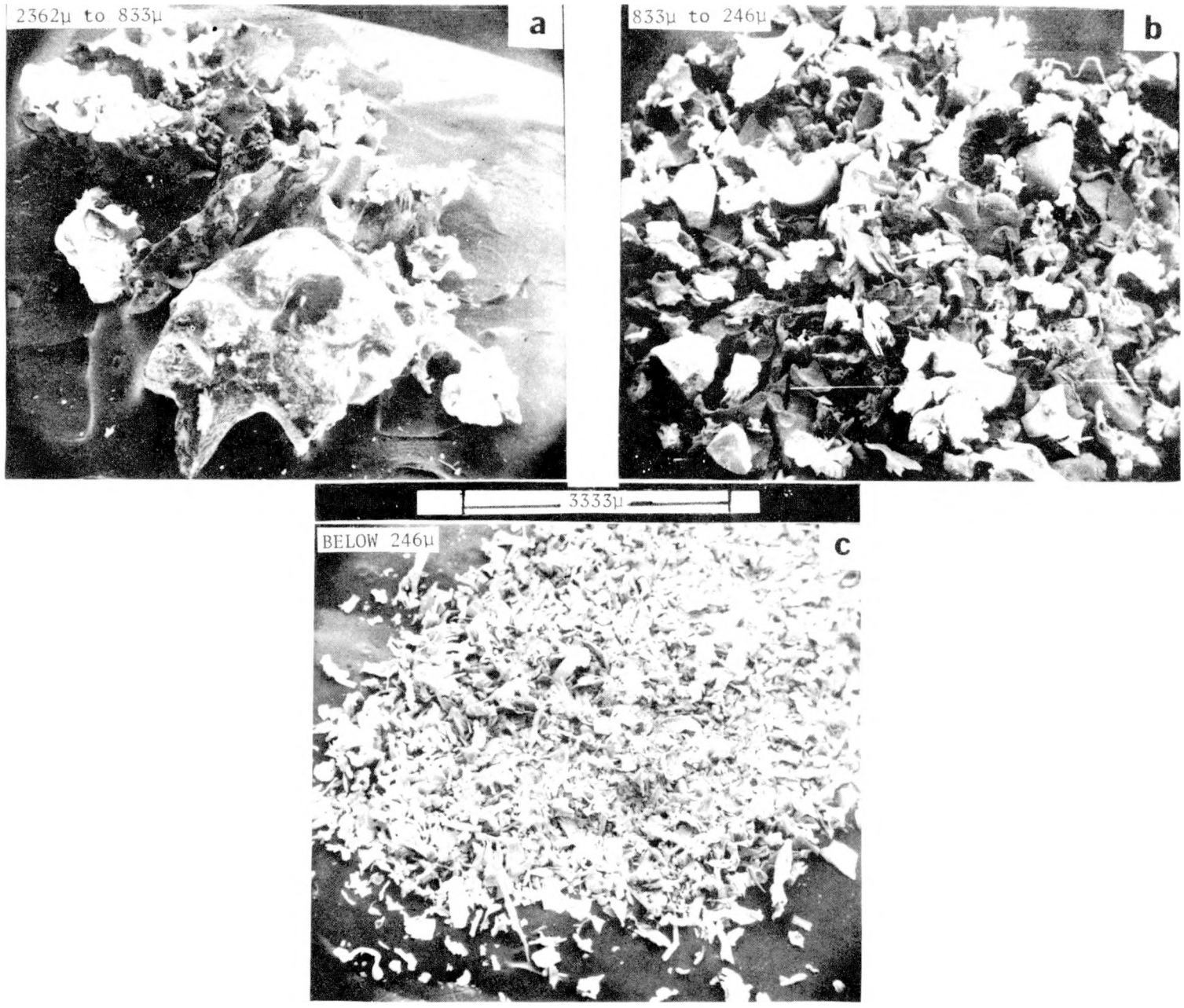

FIGURE 9. Magnified Photographs of Portions of Particles in Different Size Ranges Shown in Figure 7(B).

833 μ range are of two types; one is solidified shell type with smooth surfaces whereas the other type shows extreme porosity. The 833 μ to 246 μ particles are also seen to be of similar nature. Further examination indicated that the majority of the particles in the size range of 2,362 μ to 246 μ are of the porous type. The particles below 246 μ size range are seen in Figure 9(c) and a magnified photograph of some of the particles is shown in Figure 10(a). The particles are found to be non-spherical and also of non-porous type. The central particle in Figure 10(a) was photographed with further magnification and is seen in Figure 10(b). Cracking on this particle is quite evident and was found to be a general characteristic of many particles which made them very fragile.

Details of the porous structure of the particle in the upper left corner of Figure 9(a) are shown in Figure 11. It is clear that the porosity is of extremely fine scale.

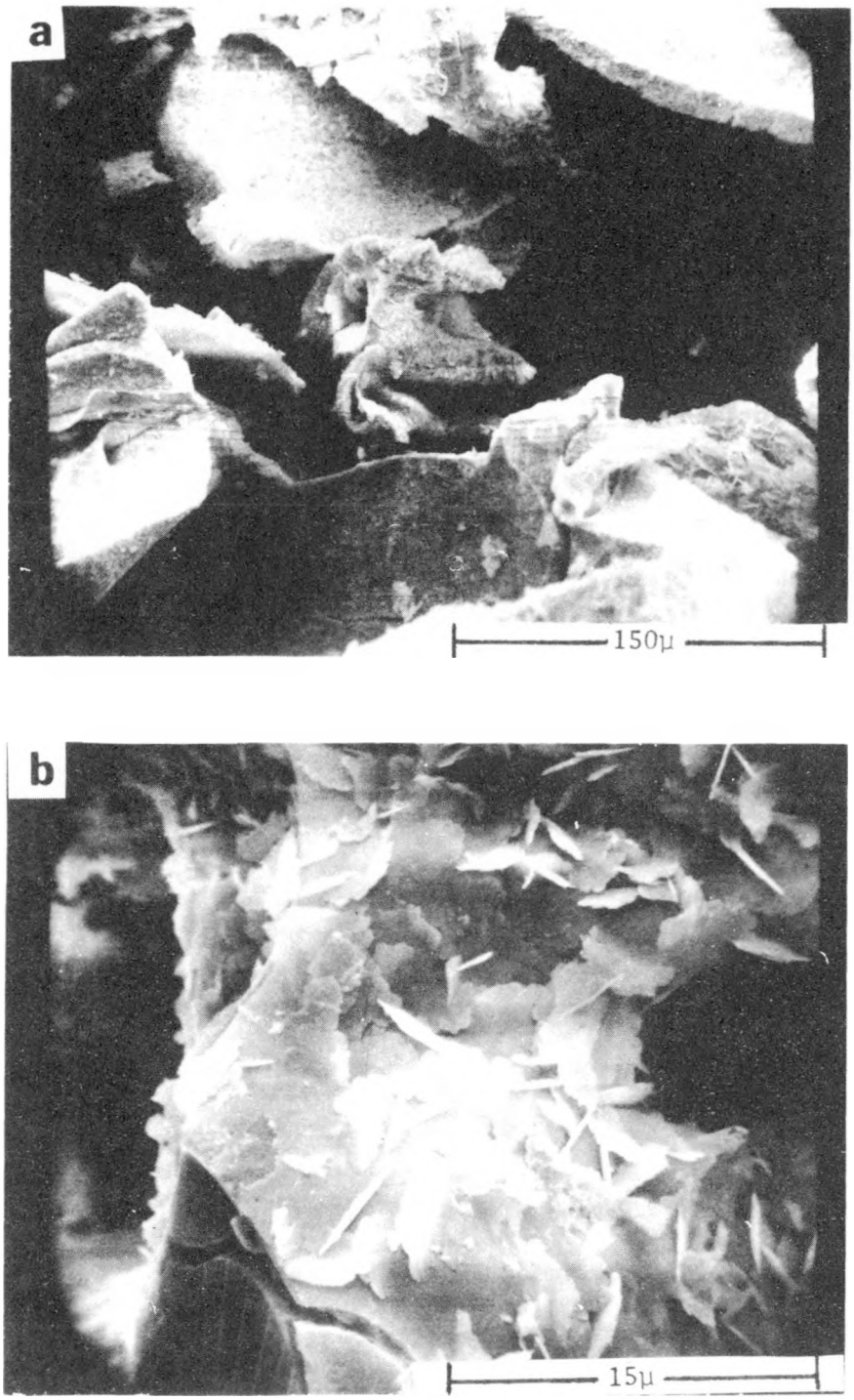

FIGURE 10. Magnified Photograph Illustrating the Porous Structure of a Particle in the Size Range 2,362 μ to 833 μ Shown in Figure 9(a).

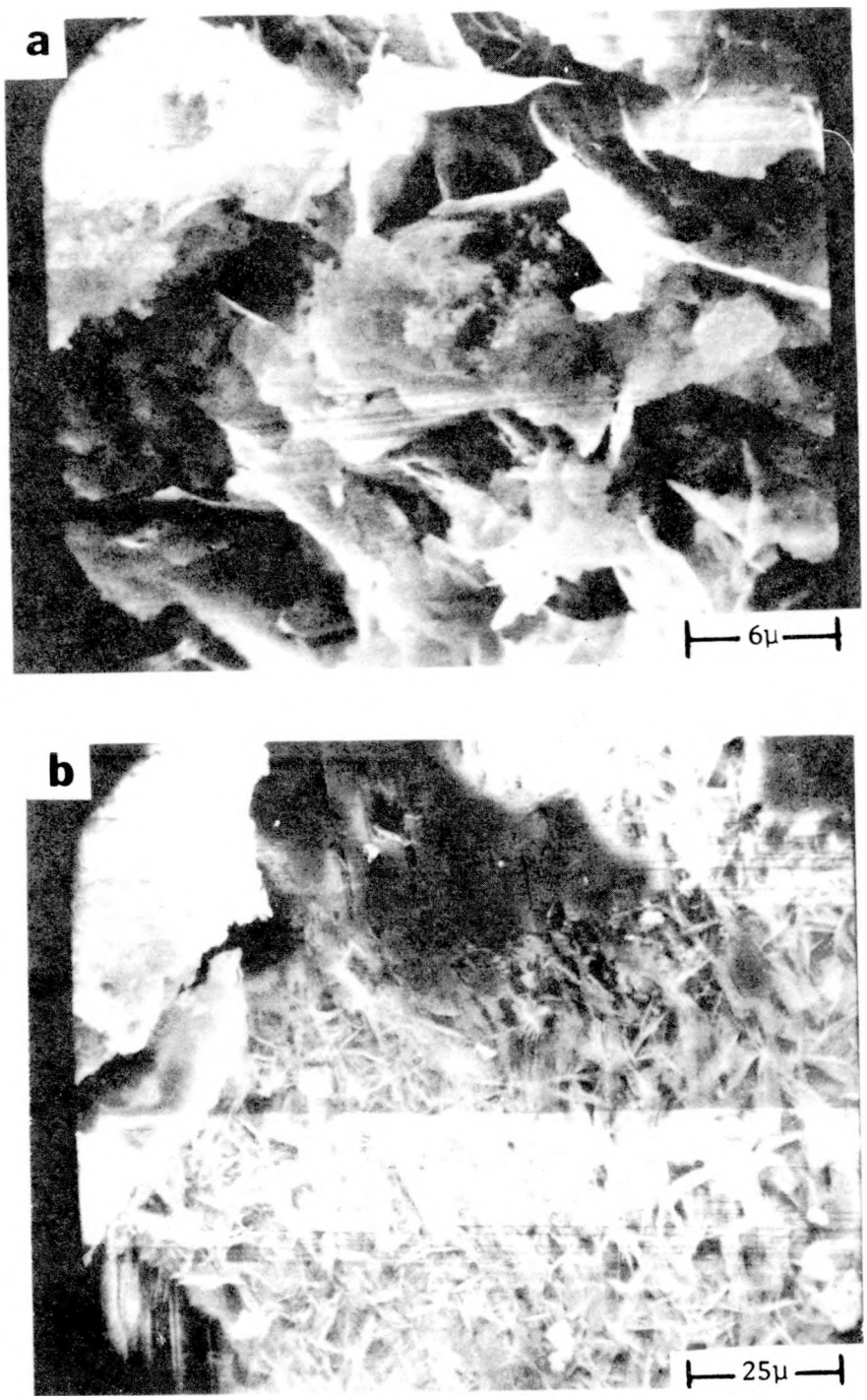

FIGURE 11. Details of the Porous Structure of the Particle in the Upper Left Corner of Figure 9(a).

IV. DISCUSSION OF RESULTS

From Table 2, it may be seen that for the molten glass/water combination, the predicted temperature for film boiling (∿420° C) is considerably lower than the melting temperature of glass (∿750° C). Thus, it may be expected that prior to breakdown of the vapor film, molten glass would begin to solidify, thus preventing an energetic interaction. This explains, perhaps, the little breakup of observed of molten glass dropped into water under "natural" free fall conditions as seen in Figure 5(A). However, the final product was extremely fragile owing to extensive internal cracking and if not handled carefully, the final product would have crumbled into smaller pieces. The internal cracking may have occurred as a result of slowly cooled solidification in the film boiling regime or as a result of rapid cooling of the solidified glass subsequent to the film breakdown. It is of interest to point out here, that Cronenberg et al. [13], have shown that behavior of the thermal stress phenomenon in a solidifying sphere is considerably different for low thermal diffusivity materials such as UO_2 as compared to this behavior for higher thermal diffusivity materials such as metals. Present results seem to support their calculations in the sense that molten glass which tends to freeze in the film boiling regime does show intensive internal cracking; whereas molten aluminum, which also tends to solidify in the film boiling regime under natural free fall conditions, does not show internal cracking.

Under forced contact, conditions, on the other hand, molten glass does energetically interact with water, resulting in extensive fragmentation (Figures 5(C) and 7(B)). Present observations of the glass/water interaction show many similarities with experimental observations

of tin/water interaction by several investigators [2, 5, 6]. Some of the similarities are noted below:

(a) A single event is observed to consist of multiple interactions with growth and collapse cycles (Figures 6 and 7(A)).

(b) Successive new interactions are triggered upon collapse of the preceding interaction (Figure 6).

(c) Growth times of a single interaction are observed to be of the order of two to three milliseconds (Figures 6 and 7(A)).

(d) Final debris shows extensive fragmentation with many particles in the middle size range (2,362 μ - 246 μ) having porous structure (Figures 9 and 11).

These similarities show that many physical characteristics of a fuel/coolant interaction, as proposed in the cyclic growth model of Buchanan et al. [5], are also present for a fuel/coolant combination in which fuel is a low thermal diffusivity material and commencement of solidification of the fuel is predicted upon liquid/liquid contact. The similarities, in addition, show that the fragmentation mechanism for molten glass contacting water is essentially the same as the fragmentation mechanism for molten tin contacting water. Since the fragmentation of tin in water cannot be of a thermal stress origin, one may conclude on the basis of present findings, that fragmentation originating from a thermal stress mechanism plays only a minor role in fragmentation of glass in water.

Thus, we have observed an energetic interaction (growth times of the order of a few milliseconds) with a fuel/coolant combination which simulates the thermal characteristics of UO_2/sodium combination quite well. In addition, the particle size distribution of the final debris

from glass/water interactions are observed to be coarser than the UO_2/sodium interactions (Figure 8). From the above findings we may expect UO_2/sodium interactions to be energetic in nature with the appropriate contact conditions, contrary to some experimental observations.

The contradiction may show either of the following:

(i) The particle size distribution curve for the glass/water interaction shown in Figure 8 should be shifted to the right to compensate for the porosity of many fragmented particles, or

(ii) The particle size distribution range for UO_2/sodium interactions shown in Figure 8 should be moved to the left to compensate for additional break-up of particles which may have occurred during the retrieval and analysis phases for the fragmented UO_2 particles.

It has been observed [12] that fragmented UO_2 particles are extremely fragile, as also observed for fragmented glass particles. However, analysis of fragmented UO_2 particles present in a sodium bath requires elaborate procedures [14], whereas it was a relatively easy procedure for the measurement of glass particles present in a water bath.

In any case, present glass/water interaction findings coupled with the comparison shown in Figure 8, suggests that basic mechanisms for UO_2 fragmentation in sodium are the same as those for glass fragmentation in water. However, the contact conditions tested to date may not be favorable for an energetic UO_2/sodium interaction.

V. CONCLUSIONS

Experimental results are presented for the thermal interaction of molten glass with water under both natural and forced free fall conditions. Extensive fragmentation was observed for forced contact conditions. Multi-flash photographs of the event indicated interactions to be of an energetic nature, with growth times to be of the order of a few milliseconds. In addition, multiple interactions were observed to exist within a single event and a new interaction was triggered upon the collapse of the previous one. These findings are very similar to tin/water interaction observations and lend support to the cyclic theory of bubble growth and collapse proposed by Buchanan et al. [5] for fuel/coolant interactions.

Contrary to the tin/water interaction studies, present observations are for a fuel/coolant combination with simulates thermal characteristics of UO_2/sodium considerably more accurately. The thermal diffusivity of molten glass is on the same order as the thermal diffusivity of UO_2 and for the molten glass/water combination the predicted interface temperature is considerably lower ($\sim$175° C) than the melting temperature of glass. The latter prediction is also true for the UO_2/sodium combination.

Particle size distributions of the final debris from the glass/water interaction was found to be on the coarse side when compared to the particle size distribution for the final debris from some in-pile and out-of-pile UO_2/sodium interactions. The discrepancy raises questions concerning whether all of the possible contact modes between UO_2/sodium are covered in the experiments to date. In particular, the mode of contact not tested is where molten UO_2 enters a sodium bath in the film boiling regime (at least as predicted by Henry's correlation) and soon after entry a forcible collapse of vapor is achieved between UO_2 and sodium by external means.

REFERENCES

1. Caldarola, L., "Current Status of Knowledge of Molten Fuel/Sodium Thermal Interactions," KFK-1944, Kernforshunzszentrum, Karlsruhe, February 1974.

2. Arakeri, V. H., et al., "An Experimental Study of the Thermal Interaction for Molten Tin Dropped into Water," UCLA-ENG-7592, University of California, Los Angeles, December 1975.

3. Morey, L. W., The Properties of Glass, 2nd Ed., Reinhold, New York, 1954.

4. Henry, R. E., "A Correlation for the Minimum Film Boiling Temperature," Proc. of AICHE Heat Transfer Conference, Atlanta, 1973.

5. Buchanan, D. J. and Dullforce, T. A., "Fuel-Coolant Interactions/Small-Scale Experiments and Theory," Second Specialist Meeting on Sodium Fuel Interaction in Fast Reactors, ISPRA, November 1973.

6. Board, S. J., Farmer, C. L., and Poole, D. H., "Fragmentation in Thermal Explosions," Int. J. Heat Mass Transfer, Vol. 17, p. 331, 1974.

7. Plesset, M. S. and Chapman, R. E., "Collapse of an Initially Spherical Vapor Cavity in the Neighborhood of the Solid Boundary," J. Fluid Mech, Vol. 47, p. 243, 1971.

8. Buchanan, D. J., "Penetration of a Solid Layer by a Liquid Jet," J. of Phys. D., Appl Phys. 6, p. 1,762, 1973.

9. Cronenberg, A. W. and Fauske, H. K., "UO_2 Solidification Phenomenon Associated with Rapid Cooling in Liquid Sodium," J. Nucl. Matr., 52, p. 24, 1974.

10. Proc. 3rd Internat. Congr. Acoustics, 1959, Part 1, pp. 321-329, Elsevier Publishing Co., 1961.

11. Chace, W. O. and Moore, H. K. (Eds.), Exploding Wires, Vol. 1, Plenum Press, Inc., New York, 1959.

12. Mizuta, H., "Fragmentation of Uranium Dioxide after Molten Uranium Dioxide-Sodium Interaction," J. of Nuc. Sci. and Techn., Vol. 11, p. 480, November 1974.

13. Cronenberg, A. W., Chawla, T. C., and Fauske, H. K., "A Thermal Stress Mechanism for the Fragmentation of Molten UO_2 upon Contact with Sodium Coolant," Nucl. Eng. and Design, Vol. 30, p. 434, 1974.

14. Henry, R. E., et al., "Large Scale Vapor Explosions," Proc. of ANS Conf. on Fast Reactor Safety, Los Angeles, p. 922, 1974.